Electronic Supplementary Material (ESI) for Physical Chemistry Chemical Physics.

Supplementary Information

Conformation-induced separation of 3-chloropropene from 1-chloropropane through nanoporous monolayer graphenes

Yinxiang Xu[a,b,c], Yujia Zhang [c,d], Steven Wang[e], Junbo Xu[c,*] and Chao Yang [a,c,d,*]

[a] School of Space and Environment, Beihang University, Beijing 100191, China

[b] College of Mechanical Engineering, Sichuan University of Science and Engineering, Sichuan 643000, China

[c] CAS Key Laboratory of Green Process and Engineering, Institute of Process Engineering, Chinese Academy of Sciences, Beijing 100190, China

[d] University of Chinese Academy of Sciences, Beijing 100190, China

[e] School of Engineering, Newcastle University, NE1 7RU, UK

[*] Corresponding authors: jbxu@ipe.ac.cn (J.B. Xu); chaoyang@ipe.ac.cn (C. Yang)

Section I. Properties of hydrocarbon molecules and membranes

Table S1. Properties of C_3H_7Cl and C_3H_5Cl

	Diameter [a] (Å)	Dipole (debye)	Boiling point (°C)	Critical temperature (°C)	Critical pressure (MPa)
C_3H_7Cl	5.26	2.11	46.60	230.00	4.58
C_3H_5Cl	5.13	1.94	45.00	241.00	4.76
C_3H_8	4.92	0.06	-42.09	96.80	4.25
C_3H_6	4.76	0.41	-47.40	91.61	4.60

[a] Molecular diameter is the equivalent diameter when a hydrocarbon molecule with the vdW surface was treated as a sphere.

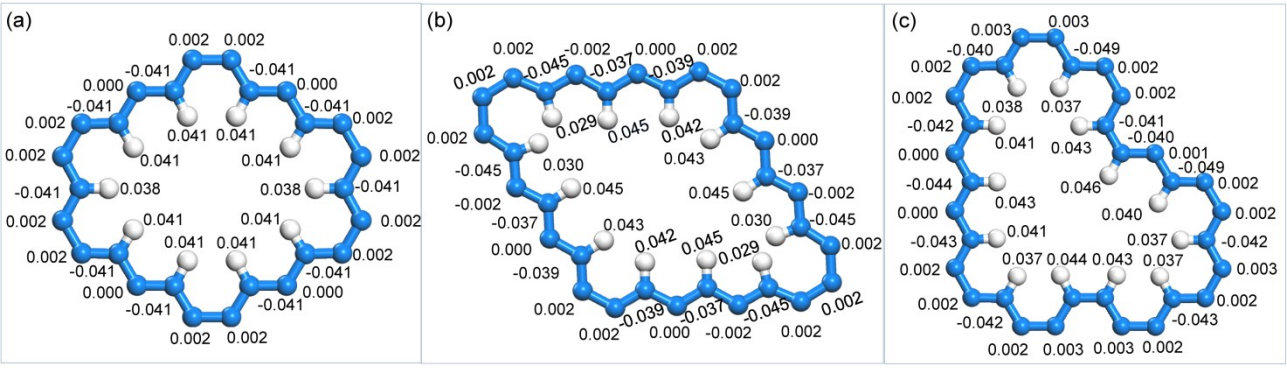

Figure S1. Atomic charges of (a) H-pore-16, (b) H-pore-18 and (c) H-pore-21 from Hirshfeld charge analysis. (Only the atoms close to the pores are shown for clarity; C, blue; H, white).

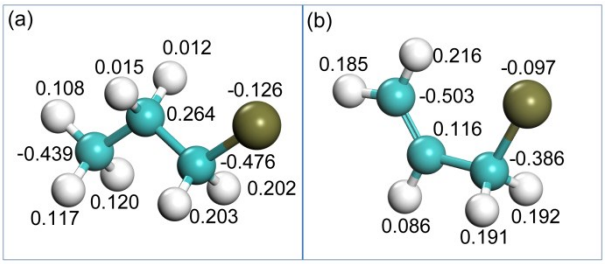

Figure S2. ESP charge distributions of (a) C_3H_7Cl and (b) C_3H_5Cl from DFT calculations

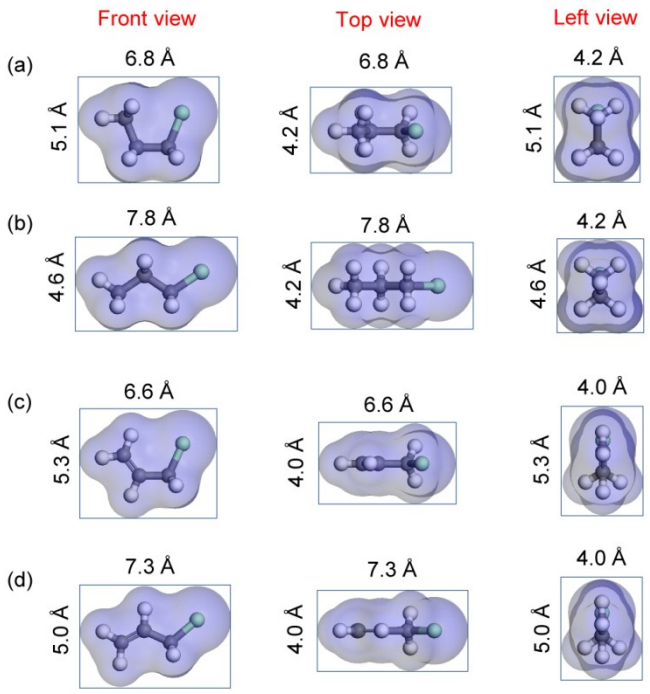

Figure S3. Three views of C_3H_7Cl and C_3H_5Cl at different Cl-C-C-C dihedral angles: (a) C_3H_7Cl (0^o), (b) C_3H_7Cl (180^o), (c) C_3H_5Cl (0^o) and (d) C_3H_5Cl (180^o). The vdW scale factor is 1.0.

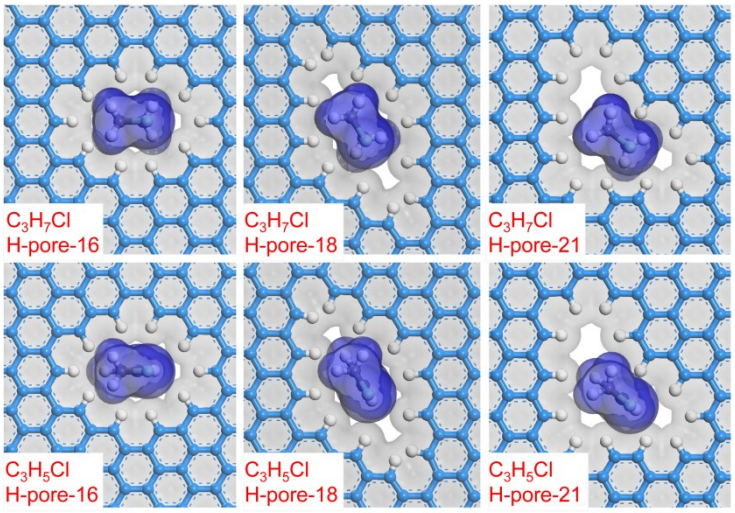

Figure S4. Complementarity diagrams of rigid H-pore-16, H-pore-18 and H-pore-21 membranes with cis-C_3H_7Cl and cis-C_3H_5Cl in the left view in Figure S3. It seems that the sizes of both molecules are slightly bigger than that of the pores, which may restrict them to cross the pores. But take note that the H atoms and the first C layer close to the pore are flexible during the MD simulation, which can

influence the real compatibility. Meanwhile, the local three-dimensional sizes of hydrocarbon molecules are different, and the molecular flexibility can help the residues hurdle across the single-layer NG membrane step by step, other than penetrating straightly.

Table S2. Pore sizes of the nanoporous graphene membrane in this study

Parameters	H-pore-16	H-pore-18	H-pore-21
l^a (Å)	5.56	7.87	6.84
s^a (Å)	3.88	3.89	3.88
pore size[a] (Å)	4.77	5.88	5.36

[a] Pore size of those models was characterized as the average of the shortest (*s*) and largest (*l*) in the pore with the vdW surface

Section II. Simulation results

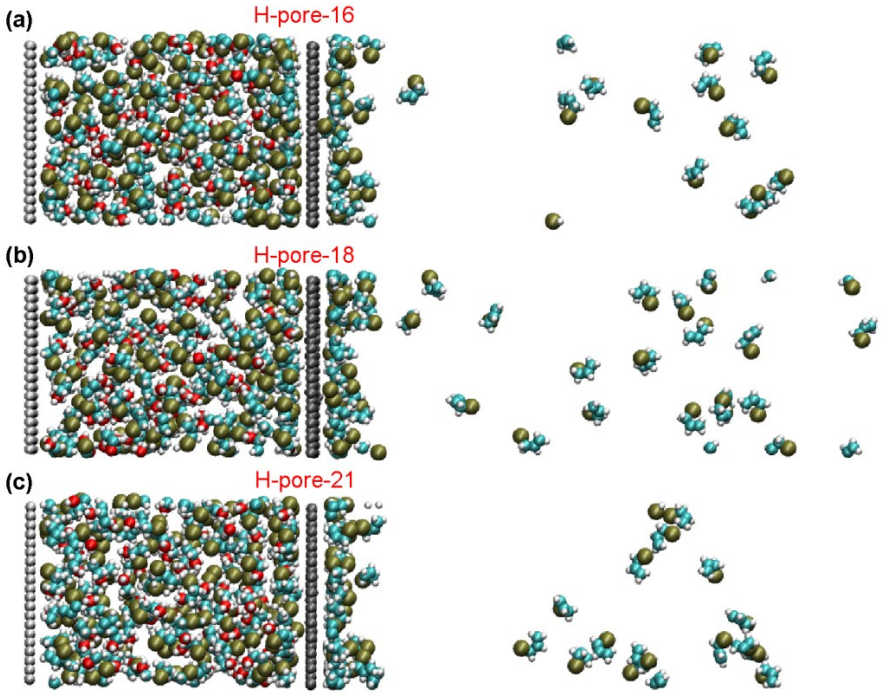

Figure S5. Snapshots of penetrated molecules passing through H-pore-16, H-pore-18 and H-pore-21 after a 100 ns MD simulation. (cyan, C in hydrocarbon molecules; black, C in the monolayer graphene; milk white, He; white, H; tan, Cl; red, the marked C of C_3H_7Cl)

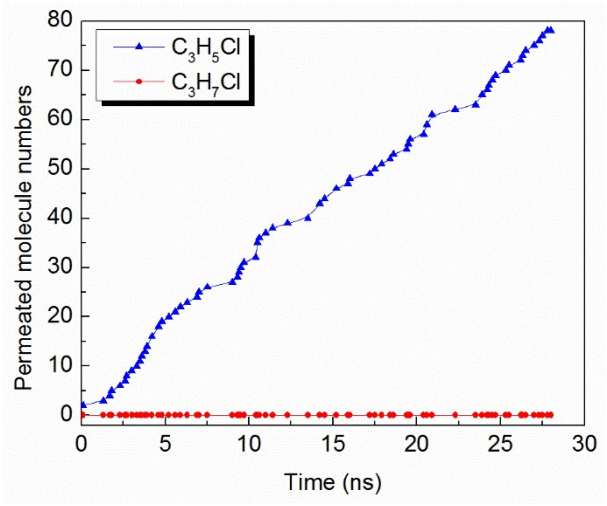

Figure S6. Permeated molecule numbers of 800 C_3H_5Cl and 800 C_3H_7Cl in 2×2×2 supercells penetrating the H-pore-16 NG membranes with four pores for a 28-ns MD simulation. No C_3H_5Cl crossing events take place.

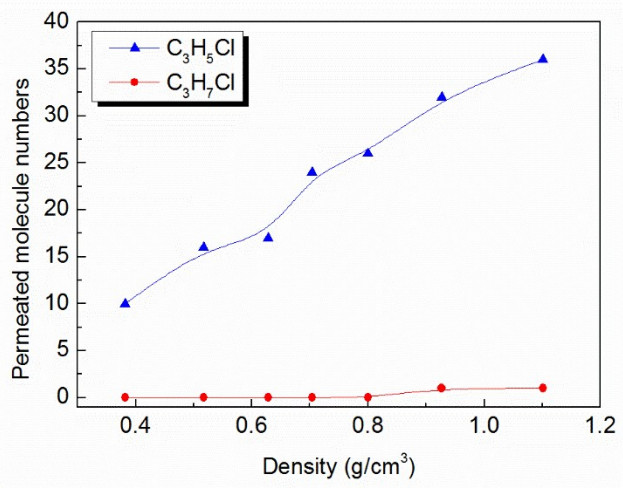

Figure S7. Permeated molecule numbers of C_3H_5Cl and C_3H_7Cl passing through H-pore-16 as a function of initial densities in the molecular chamber after 30-ns MD simulations. The He wall in the simulation box was set as impermeable and movable piston to push the mixtures toward/backward the NG membrane, which can increase/decrease the initial molecular densities of the molecule chamber. To study the effects of the pressures on penetration behaviors, the NEMD simulations were performed for 30 ns to collect the data at different displacements (-40 Å~10 Å) of the movable He wall.

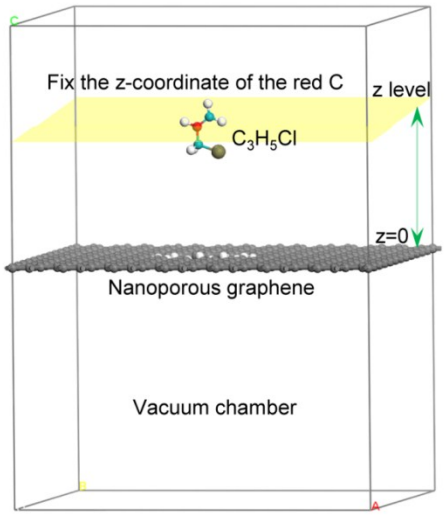

Figure S8. Simulation box of a hydrocarbon molecule passing through the pore. The molecule can three-dimensionally rotate, twist, and move in a given *z* level by only controlling the *z*-coordinate of the middle C (red) in a hydrocarbon molecule to screen the conformations with lower interaction energy between the molecule and nanoporous graphene.

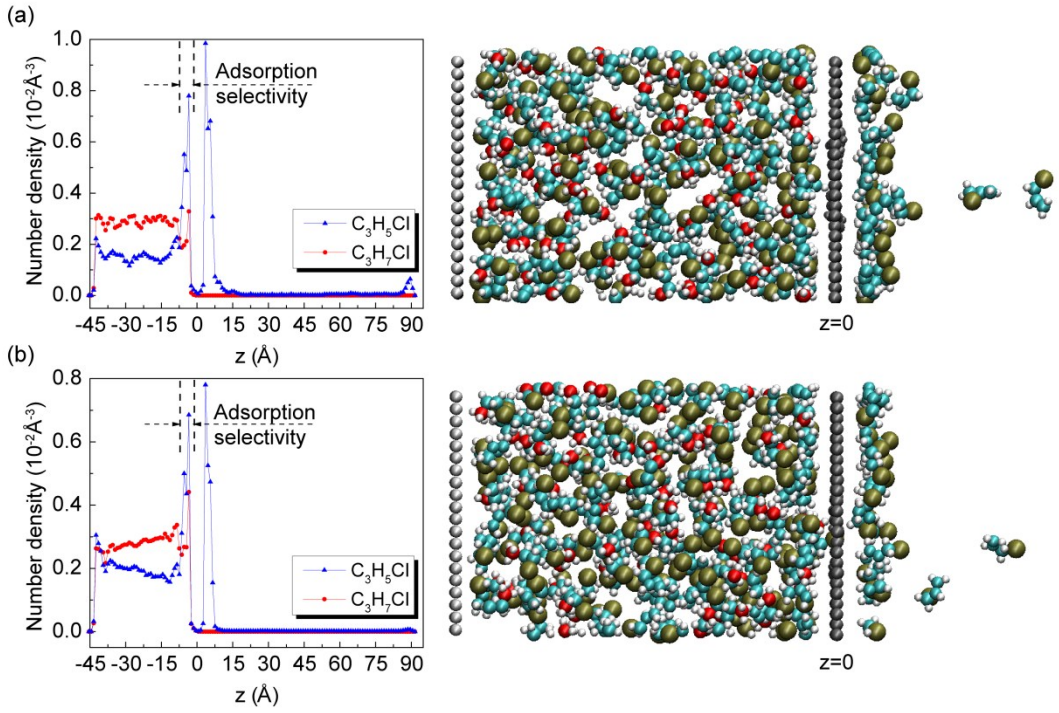

Figure S9. Average number density profiles of C_3H_5Cl and C_3H_7Cl (marked with the red C) molecules passing through (a) H-pore-18 and (b) H-pore-21 along *z* axis during the 30-31 ns MD simulation where data were collected every 10 fs, and the corresponding snapshots during the MD simulation.

Table S3. The average molecule number of C_3H_5Cl/C_3H_7Cl in the adsorption layer ($-6.5<z<-2.4$) for 1 ns and the adsorption selectivity

NG membranes	Average molecular numbers		Adsorption selectivity [a]
	C_3H_7Cl	C_3H_5Cl	
H-pore-16	7.91	20.51	2.59
H-pore-18	8.22	19.36	2.36
H-pore-21	10.95	17.23	1.57

[a] Adsorption selectivity is defined as the adsorbed molecule ratio of C_3H_5Cl to C_3H_7Cl in the adsorption layer.

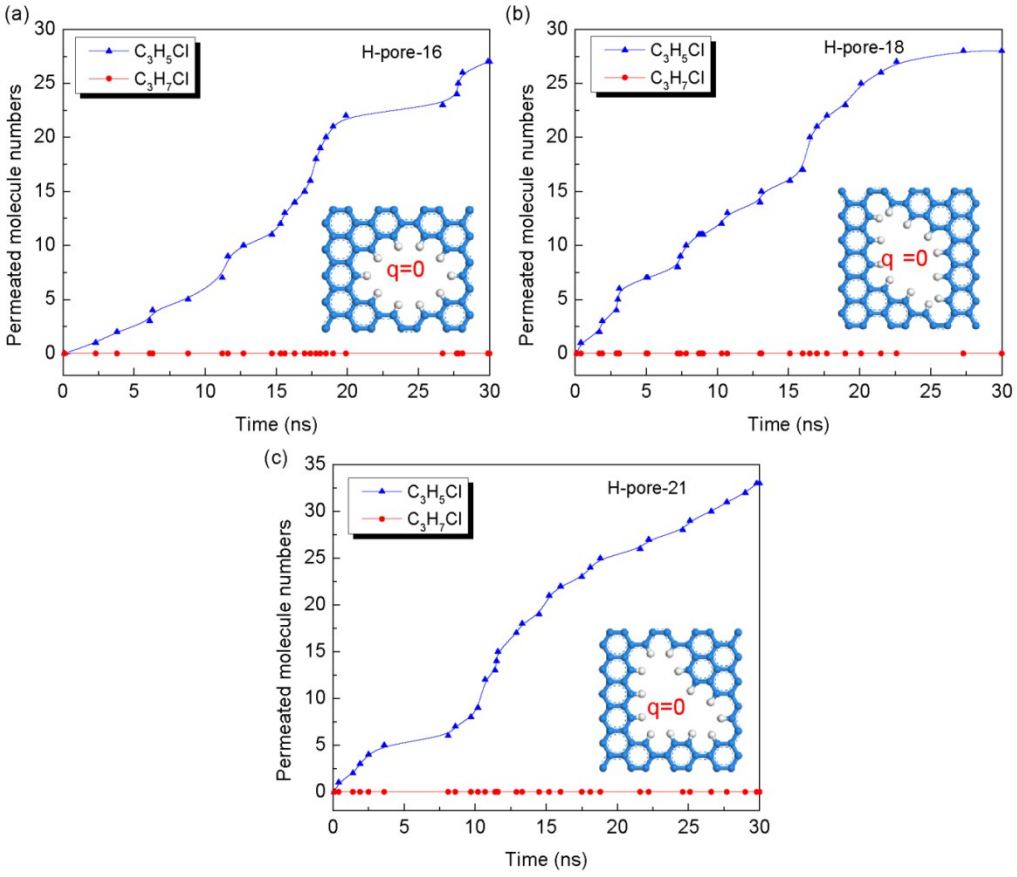

Figure S10. Separation performances of nanoporous graphenes with all atoms charged 0: (a) H-pore-16, (b) H-pore-18 and (c) H-pore-21. Only C_3H_5Cl can pass through the pores.

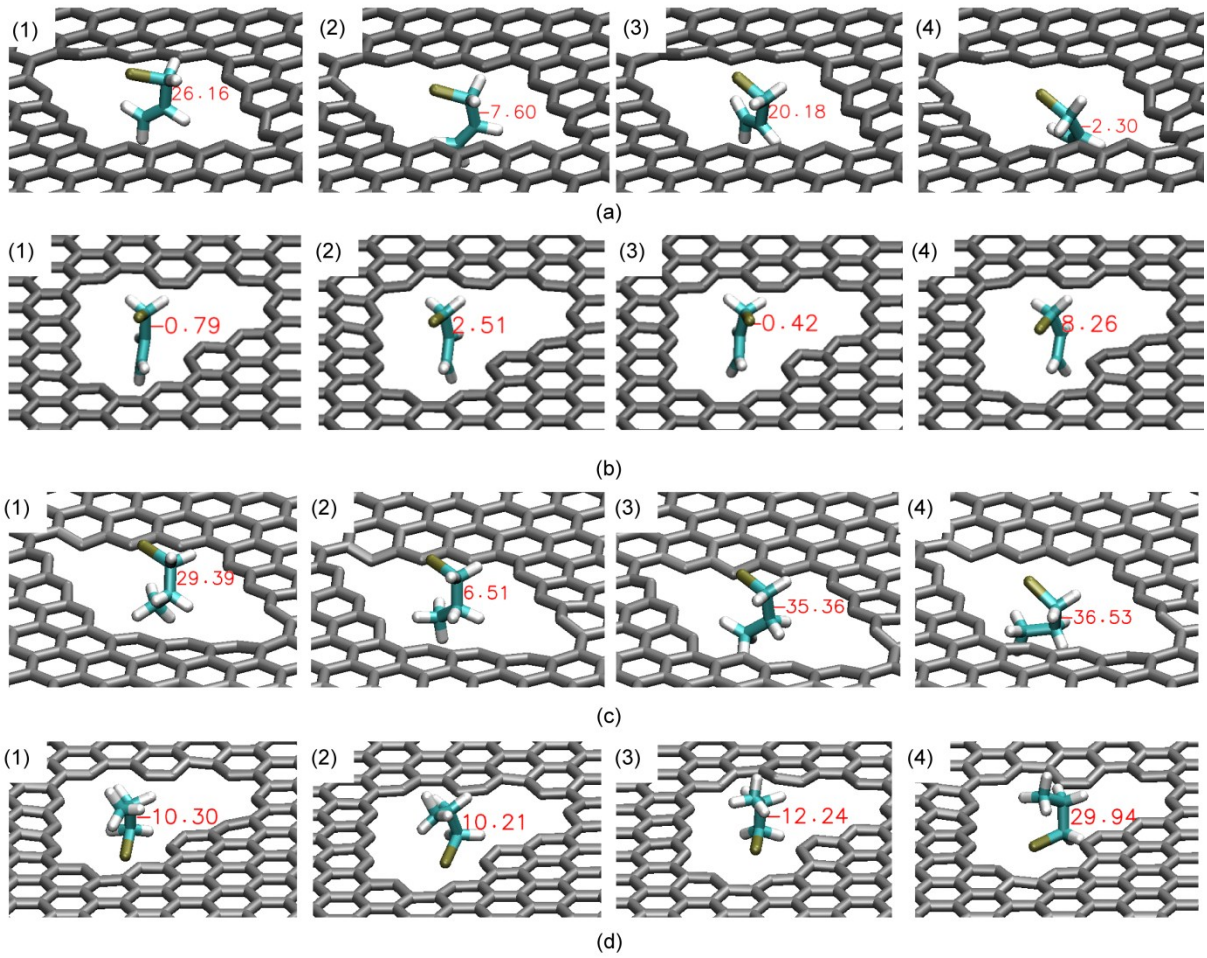

Figure S11. Snapshots of C_3H_5Cl crossing (a) H-pore-18 and (b) H-pore-21 obtained from the NEMD simulation; and snapshots of C_3H_7Cl forced to pass through (c) H-pore-18 and (d) H-pore-21 under a high initial density by pushing the He wall toward the NG membrane. During the simulation, we also found that ultrahigh pressures may result in the severe deformation of flexible pores, which may weaken the conformation recognition ability of pores. The Cl-C-C-C dihedral angles of hydrocarbon molecules were labeled in the figures. For clarity, the H atoms on the graphene membranes were not displayed.

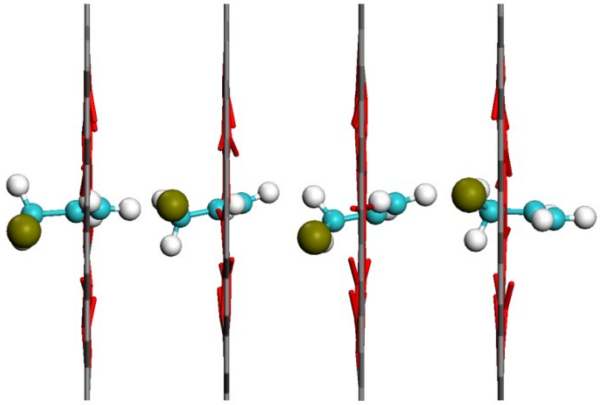

Figure S12. Side views of C_3H_5Cl crossing the H-pore-16 membrane obtained from the NEMD simulation (red, the H atoms and the first C layer around the pore; black, the fixed C atoms in the membrane). It can be found that the pore structure was affected by the fluctuations of dangling H atoms, thus influencing the molecule/pore compatibility in Figure S4 (rigid pore). In the actual applications, there may be underlying supporting membranes and the suspended C-H bonds in the separation membrane may have a large flexibility. Thus, freezing all the atoms in the membrane may lead to unrealistic C-C-H bond angles and the flexible pore is more close to the real condition.

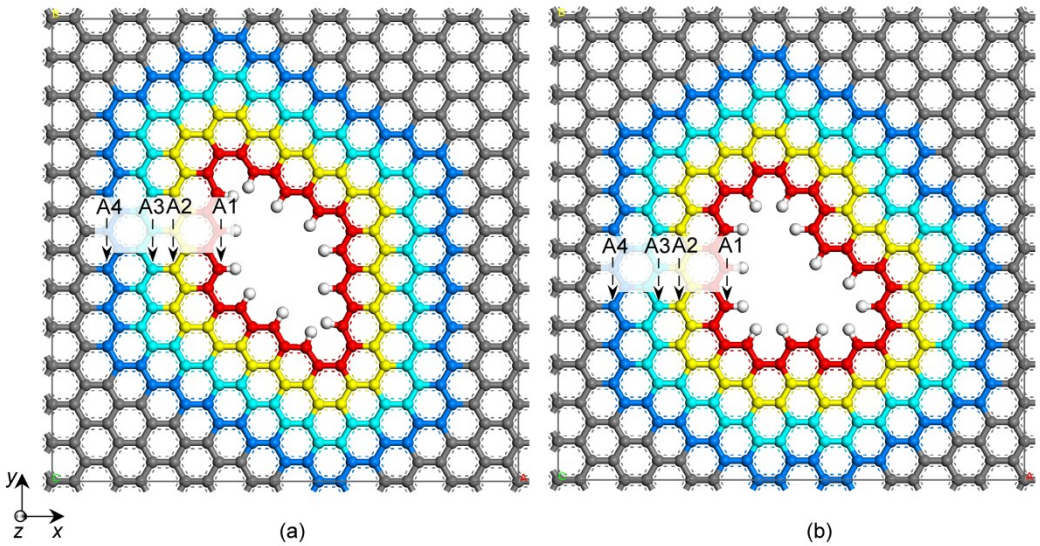

Figure S13. Honeycomb models of relaxing H atoms and 1~4 carbon layers around the pore in (a) H-pore-18 and (b) H-pore-21 during the NEMD simulation. Inserts represent the carbon atoms in different flexible layers along the *x* direction.

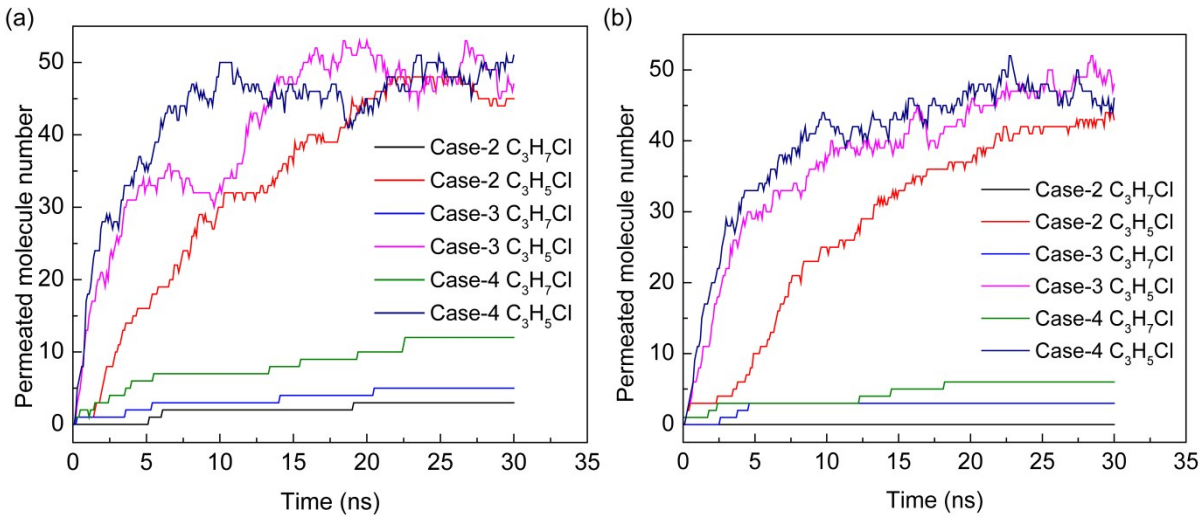

Figure S14. Number of permeated C_3H_5Cl/C_3H_7Cl molecules through the H-pore-18 and H-pore-21 membranes with 2~4 carbon layers around the pore relaxed during 30-ns NEMD simulations where 100 C_3H_5Cl and 100 C_3H_7Cl molecules were initially placed in the chamber with the volume of 29.82 × 29.52 × 85.54 $Å^3$.

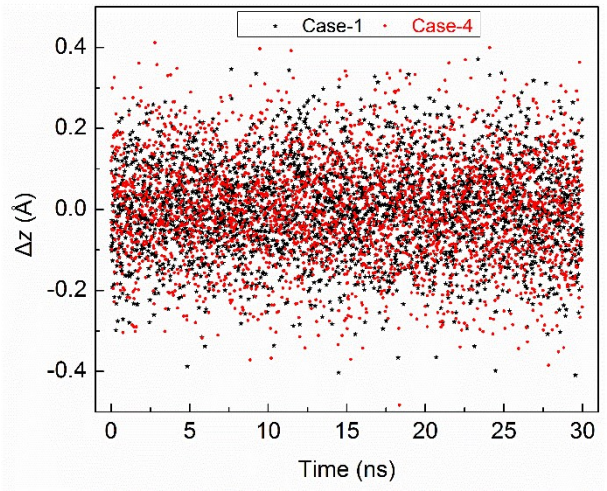

Figure S15. The recorded displacements of the atom A1 at the pore edge in the H-pore-16 membrane with the relaxation of 1-layer carbon neighbors (Case-1) and 4-layer carbon neighbors (Case-4) during the simulation (3000 points every case) along the *z* direction (as an example).

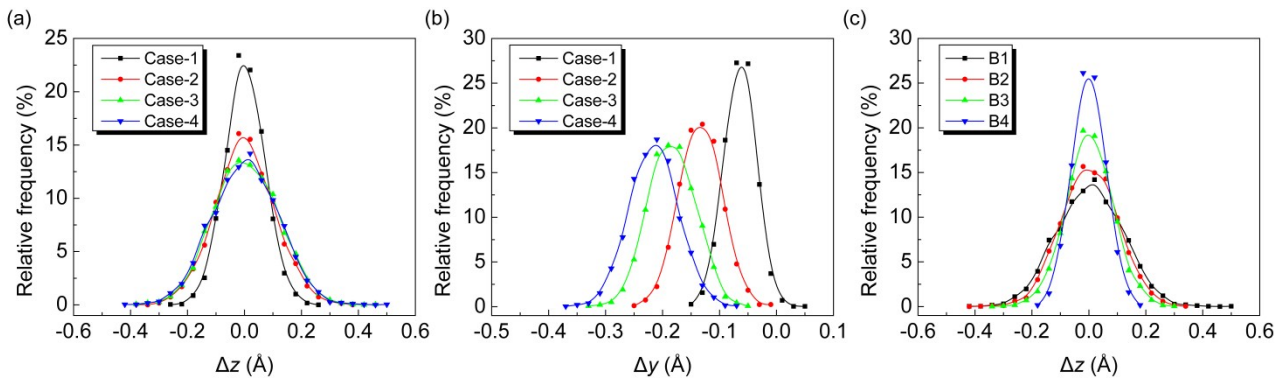

Figure S16. Frequency distributions for the displacements of the carbon atom B1 in the H-pore-16 membrane compared with the initial positions in different cases during 30-ns NEMD simulations: (a) along the *z* direction and (b) along the *y* direction; (c) frequency distributions for the displacements of the carbon atoms B1~B4 along the *z* direction in Case-4.

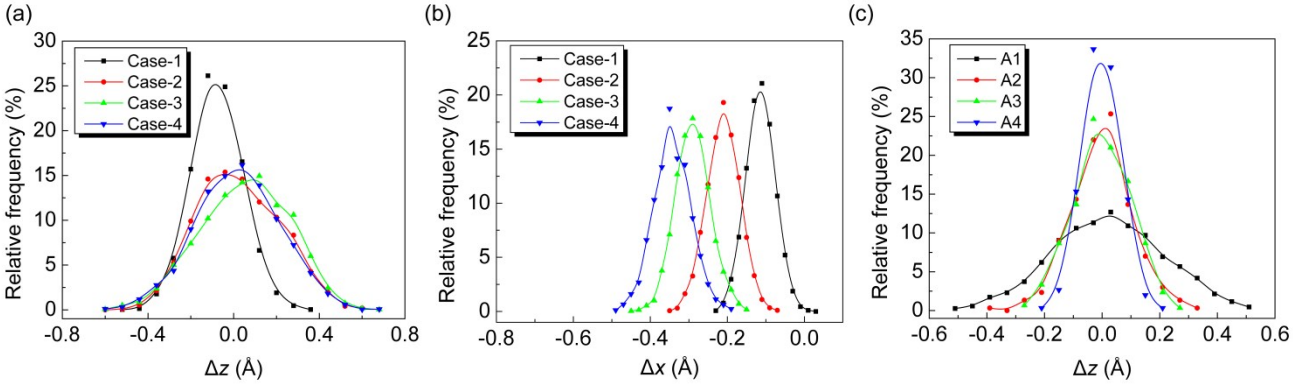

Figure S17. Frequency distributions for the displacements of the carbon atom A1 in the H-pore-18 membrane compared with the initial positions in different cases during 30-ns NEMD simulations: (a) along the *z* direction and (b) along the *x* direction; and (c) frequency distributions for the displacements of the carbon atoms A1~A4 along the *z* direction in Case-4.

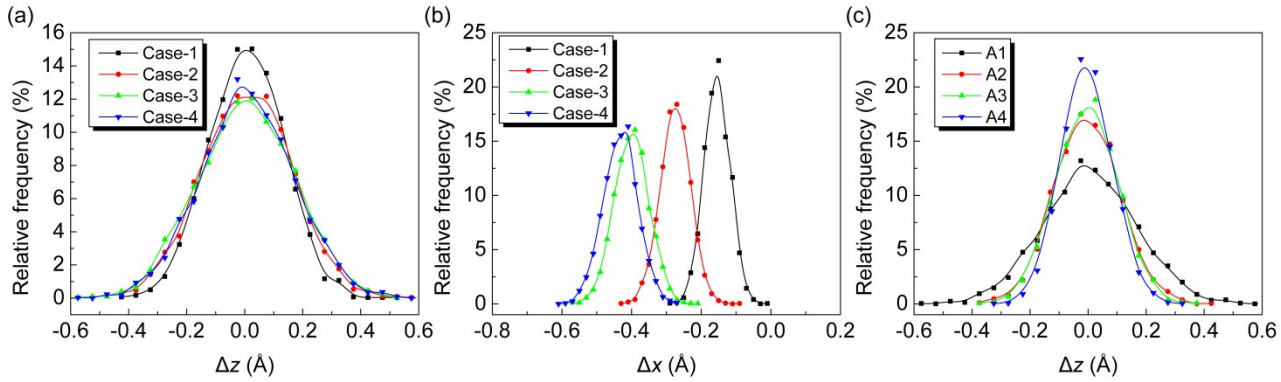

Figure S18. Frequency distributions for the displacements of the carbon atom A1 in the H-pore-21 membrane compared with the initial positions in different cases during 30-ns NEMD simulations: (a) along the *z* direction and (b) along the *x* direction; (c) frequency distributions for the displacements of the carbon atoms A1~A4 along the *z* direction in Case-4.